View metadata, citation and similar papers at core.ac.uk
brought to you by CORE
provided by DCU Online Research Access Service

JOURNAL OF NANOSCIENCE LETTERS

Effect of high temperature VPT conditions on the development of aligned ZnO nanorod arrays grown by a three step catalyst-free method

R. Fath Allah[a,*], D. Byrne[b], T. Ben[a], D. González[a], E. McGlynn[b], R. García[a]

[a] *Dpto. Ciencia de los Materiales e Ingeniería Metalúrgica y Q.I., Facultad de Ciencias, Apdo. 40, 11510 Puerto Real (Cádiz), Spain*
[b] *School of Physical Sciences, National Centre for Plasma Science and Technology, Dublin City University, Glasnevin, Dublin 9, Ireland*

[*] *Author for correspondence: Rabie Fath Allah, email: rabie.fath@uca.es*
Received 4 Feb 2012; Accepted 19 Mar 2012; Available Online 19 Mar 2012

Abstract

Using Transmission Electron Microscopy-related techniques, we study the effect of the high temperature in the Vapour Phase Transport (VPT) process on the morphology and chemistry of VPT ZnO nanorod arrays deposited on a two-step Chemical Bath Deposition (CBD) buffer layers on silicon substrates. Though well-aligned and *c*-axis oriented arrays of ZnO nanorods are achieved, we have noticed the strong dependence of the nanorod morphology on the VPT growth conditions such as the temperature ramp rate and the placement of samples with respect to the metal source. The development of conical structures in the nanorod bases and the formation of a double intermediate layer below the base of nanorods are the main features found. The modifications of the ZnO nanostructures both in the base and in the underlying buffer layers due to the high VPT temperatures are also examined in detail.

Keywords: ZnO nanorods array; Transmission electron microscopy; Vapour phase transport

1. Introduction

Considerable efforts have been made to fabricate low-dimensional nanostructures of zinc oxide (ZnO), since it has been recognized as a promising photonic material in the short-wavelength region with significant potential in laser emission, field emission and nanoscale heterojunctions [1]. ZnO exhibits a hexagonal structure with a direct band gap of 3.37 eV at room temperature which is very similar to that of GaN. ZnO also possesses a large exciton binding energy of 60 meV, which is much larger than that of GaN (25 meV) as well as the thermal energy at room temperature (≈ 26 meV) that can ensure an efficient exciton emission at ambient conditions [2]. ZnO is also an environmentally-friendly material that is bio-compatible, biodegradable and bio-safe for medical applications and environmental science [3, 4]. In addition to this, ZnO exhibits a vast and abundant configuration of nanostructure morphologies, such as thin films, walls, rods, belts, springs, and hemispheres [5-9], which allow the development of new electronic and optical applications. Among them, the development of 1-Dimensional structures has drawn particular interest. Recent research on ZnO nanorods extends their potential application in many devices [10, 11], such as the fabrication of Dye-Sensitized Solar Cell (DSSC) [6].

Nowadays, the growth of 1-D single crystalline ZnO nanostructures have been achieved by various growth mechanisms, such as higher temperature VPT methods (including via the vapour-liquid-solid (VLS) mechanism) (T≥900ºC) [12], thermal evaporation (1400ºC) [13] together with low temperature mechanisms such as hydrothermal growth [14] or chemical bath deposition (CBD) [7]. In particular, these CBD processes are constituted by simple solution-phase route, but it is currently difficult to control the size, density, and uniformity of the produced nanorods. Several authors have reported that the growth of ZnO nanorods via CBD is improved if the substrate is pre-seeded with ZnO crystallites [6,7,15,16]. The presence of ZnO seeds on the substrate provided a useful platform for the formation of aligned ZnO nanorods. The use of an underlying seed layer can overcome various CBD limitations, as the seed layer provides a dense network of nucleation sites with a high degree of texture, on diverse substrates, which enhances subsequent ZnO nanorod growth.

In order to combine the facility and potential benefits, (e.g. scale-up to larger substrate sizes,) of low temperature methods with the high-quality deposit obtained by high temperature growth processes, a three step catalyst-free technique has been developed, which is compatible with a variety of substrate types. In this, using low temperatures, a dense well-aligned nanorod buffer layer is grown using chemical bath deposition which is suitable for subsequent Vapour Phase Transport (VPT) deposition [17]. Morphological, compositional and structural transformations of the nanorod array during the later VPT growth stages will be analysed in detail by transmission electron microscopy (TEM) and related techniques. In particular, the final VPT rod formation and the rod structure are discussed in the light of the effects of the high temperatures typically reached during the VPT process.

2. Experimental

Highly oriented ZnO nanorods were grown on Si(111) by a simple catalyst-free method. Firstly, a thin seed layer was deposited by drop coating zinc acetate in ethanol solution after which the substrate was annealed at 350ºC in air for 30 min. This creates a thin film of aligned ZnO crystallites

© 2012 Simplex Academic Publishers. All rights reserved.

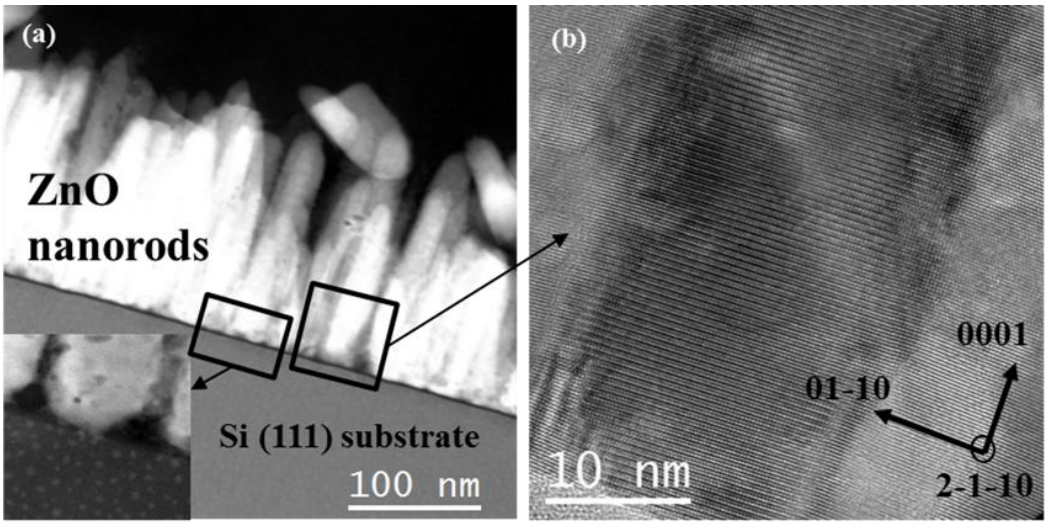

Figure 1. (a) HAADF-STEM image of ZnO nanorods in the case of sample A prepared in a common cross-sectional process. Inset a detail of the substrate ZnO rod interface. (b) HRTEM image of the rod highlighted in the square in figure a.

Table 1. Summary of experimental conditions applied on the studied samples.

	Treatments			
SAMPLE	CBD1+CBD2	(FRTP)	(FRTP2)	(SRTP)
A	X	---	---	---
B	X	X	---	---
C	X	---	---	X
D	X	---	X	---

(or seed layer, CBD1) which will act as nucleation sites during subsequent ZnO rod growth. Secondly, pre-seeded substrates were submerged in an equimolar solution of zinc nitrate and hexamethyltetramine at room temperature. The solution was heated to 90ºC and maintained at this temperature for 30 min to create a layer of aligned ZnO nanorods (CBD2). Finally, a vapour phase transport (VPT) growth step was used, where the source powder for the carbothermal reduction was prepared with a fixed amount of high purity ZnO powder mixed with high purity graphite. Samples with the two step (CBD1 + CBD2) buffer layers were placed directly above the powder source in a horizontal tube furnace and heated to 925ºC under flow of argon using both slow and a fast ramp temperature profiles, SRTP and FRTP respectively. An additional sample was grown by keeping it closer to the Zn vapour source (FRTP2). The growth methods details can be found in references [17] and [18]. Table I summarizes the samples discussed in this work. Additionally, two samples with seed and two step buffer layers have been annealed and the results analysed reveal the effect of the high temperatures used in the VPT process.

Cross-section transmission electron microscopy (XTEM) specimens were prepared using mechanical thinning and Ar^+ milling in a Gatan Precision Ion Polishing System. Additionally, we also carried out the analysis of rods scraped off the substrate and dispersed on a Cu microscope grid. The morphology and size distribution of nanorods were examined using Conventional TEM in a JEOL 1200EX microscope operating at 120 kV. The crystal structure of nanorods was analysed using high-resolution transmission electron microscopy (HRTEM) in a JEOL 2010F operating at 200 kV. The elemental analyses by scanning transmission electron microscopy (STEM) were developed in the same microscope by using the module high angle annular dark field (HAADF) and spectrometers for energy dispersive spectrometry (EDS) and electron energy loss spectroscopy (EELS).

3. Results and Discussion

3.1. Development of CBD nanorods from ZnO seeds

Prior to the VPT process, a sample (A) was examined to identify the nanorods formation following CBD on seed layers. Figure 1a shows a cross-sectional HAADF-STEM image of the nanorod structure, where the lower region corresponds to the Si substrate. Above this, nanorods are clearly revealed as brighter vertical columns. CBD rods grew in a lateral spatially confined mode due to the high density of seeds forcing good vertical alignment during the rod formation [7]. Images recorded from scratched rods reveal a bullet shape with a base width between 25-40 nm and a maximum length of 180 nm. High resolution TEM (HRTEM) mode used to study a single ZnO rod (see an example in Figure 1 b), reveals a hexagonal wurtzite ZnO crystal structure with lattice constant of c ≈ 5.2 Å, in good agreement with the standard values of bulk ZnO [19]. These results reveal the structural quality of CBD rods to be good, with no evidence of planar or other extended defects.

If we now focus on the rod/substrate interface (inset of Figure 1a), we can see just under the base of nanorods a darker region which can be related to amorphous or lower atomic number material. This layer reaches a thickness between 3 and 8 nm and its compositional distribution have been analysed along the interface by EDX spectroscopy (not shown here). High Si and O contents are revealed in the darker layer under the rods where no traces of Zn were found, defining the layer as a native oxide formed by reaction of the Si substrate.

3.2. VPT deposition on CBD nanorod buffer layer

A sample similar to sample A has been subjected to the final step of the growth process, i.e. VPT. Hereafter this new sample is referred to as sample B. Figure 2a shows a

© 2012 Simplex Academic Publishers. All rights reserved.

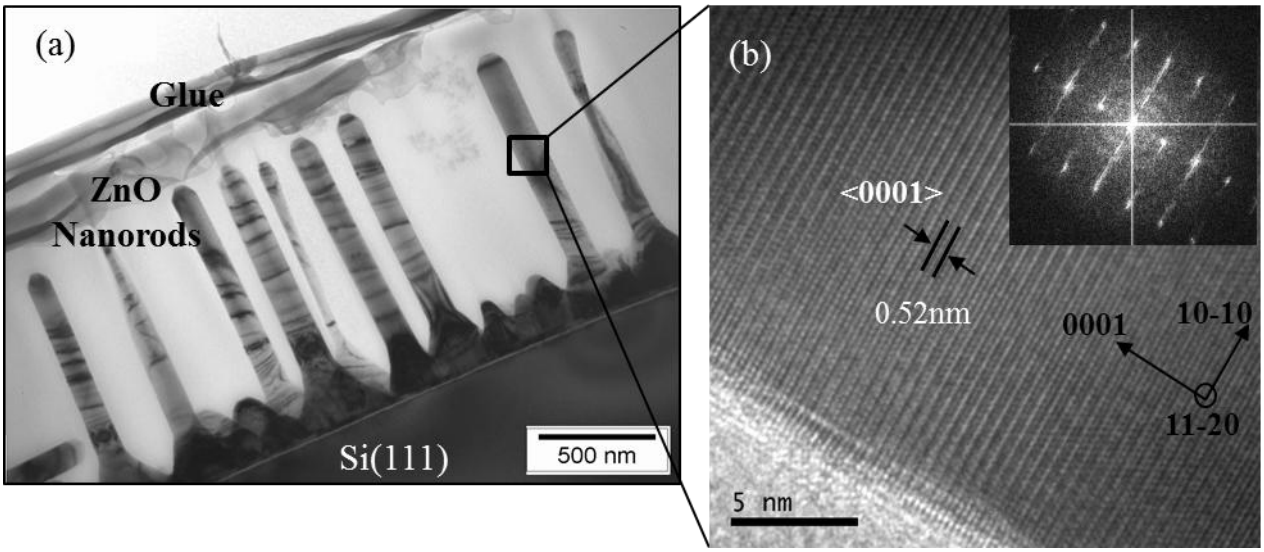

Figure 2. (a) Cross-sectional TEM image of ZnO nanorods in sample B. (b) HRTEM image confirming the high crystalline quality of the rods, inset shows corresponding FFT recorded along the [11-20] zone axis confirming the wurtzite structure and *c*-axis orientation of the nanorods.

conventional XTEM image of sample where an array of well aligned ZnO nanorods are visible, confirming the suitability of the VPT process to yield aligned nanorod structures. Intensity contrast lines observed in the rods must be related to slightly stressed condition caused by the glue used in sample preparation. Their elongated shape has clearly evolved from the CBD bullet shape where the full length measured for all VPT type rods varies between 1 to 3 µm. In this respect, rods present two clearly different areas, a conical base followed by a long body with a diamond-like facetted tip. In addition, a very good crystalline quality with well-defined atomic planes is revealed by the HRTEM image and its corresponding Fast Fourier Transform (FFT) frequency spectrum (inset of Figure 2b). In this regard, ZnO is well known to normally grow with a *c*-axis preferred orientation because of the low surface energy of the basal plane in ZnO, leading to a preferred growth in the [0002] direction [20]. However, in VPT syntheses, the growth direction of the nanorods depends on many factors such as the crystal orientation and flatness of the substrate and hence a well-aligned and *c*-oriented array of ZnO nanorods is not always achieved. In our case however, the preferential *c*-alignment is confirmed by HRTEM micrographs. The diameter uniformity along the upper section is clearly visible, with diameters around 100 nm, larger in comparison with the CBD diameters. On the other hand, the base diameters are 280-400 nm wide, very much more than the CBD diameters. From a technological point of view, an important feature of the VPT process is the significant change of the nanorod morphology giving rise to a significant transformation in the overall array. In particular, through a simple comparison we can appreciate that the nanorod density of sample B is much lower than in sample A. In fact, one VPT deposited nanorod emerges from about 80 previous CBD rods. In other words, several CBD rods have contributed to the promotion of a single VPT nanorod and then they are no longer individually distinguishable. As a result, the spacing of VPT rods is much greater than the spacing of CBD rods.

Another significant feature is the development of a complex interface between the rod bases and the substrate. In particular, cross-section views of the substrate/rod interface shown in HAADF-STEM images (see an example in Figure 3b) reveal an intermediate layer composed of two different regions with three clear interfaces. Over the crystalline silicon substrate, a darker layer with a sharp interface is visible, followed by another thicker, brighter and heterogeneous layer. Spatially resolved EEL spectra recorded across the interface evidenced the characteristic signal of the Zn-L, O-K and Si-L edges, and some individual extracted spectra are showed in Figures 3a and 3c. Just on the silicon interface, the clear change in the Si-L edge together with the appearance of the O-K peak is attributed to the formation of a SiO_2 layer (see Figure 3c points 4 and 3). The oxygen signal gradually decreases until it reaches a steady value corresponding to the onset of the ZnO nanorod (indicated as 1 in Figure 3a). However, the Zn-L signal begins before the O-K signal has reached this steady state (see point 2), i.e. before the onset of the ZnO nanorod. In this area, corresponding to the brighter layer in the HAADF-STEM image, the Zn-L edge signal does not vary significantly but the O-K signal of the recorded spectra does experience a progressive redshift when we move from the adapting layer to nanorod base (inset of Figure 3a). Moreover, in this region the Si-L edge experiences a slight change towards decreasing energies when comparing against the darker sub-layers (point 2 compared to point 3). This energy change can be explained by a ZnO/SiO_2 alloy with a band gap between the two original compounds. Such a qualitative compositional distribution has been additionally confirmed by EDX spectroscopy. These results suggest that first above the Si substrate, a SiO_2 layer is formed (darker layer), but that the brighter layer is something more than ZnO polycrystalline particles immersed in an amorphous SiO_2 matrix and that new zinc silicate species could have formed where the oxidation states of Si and Zn atoms remain constant. In this sense, FFT reconstructions of HRTEM images for several SiO_2-ZnO interfaces reveal the existence of intense spots with interplanar spacing in agreement with the values for Zn_2SiO_4 crystals. Taking into account all the EELS, EDX and HRTEM data, we conclude that the brighter and heterogeneous layer contains a mixture of ZnO and SiO_2 where they combine to form inclusions of Zn_2SiO_4 phase.

© 2012 Simplex Academic Publishers. All rights reserved.

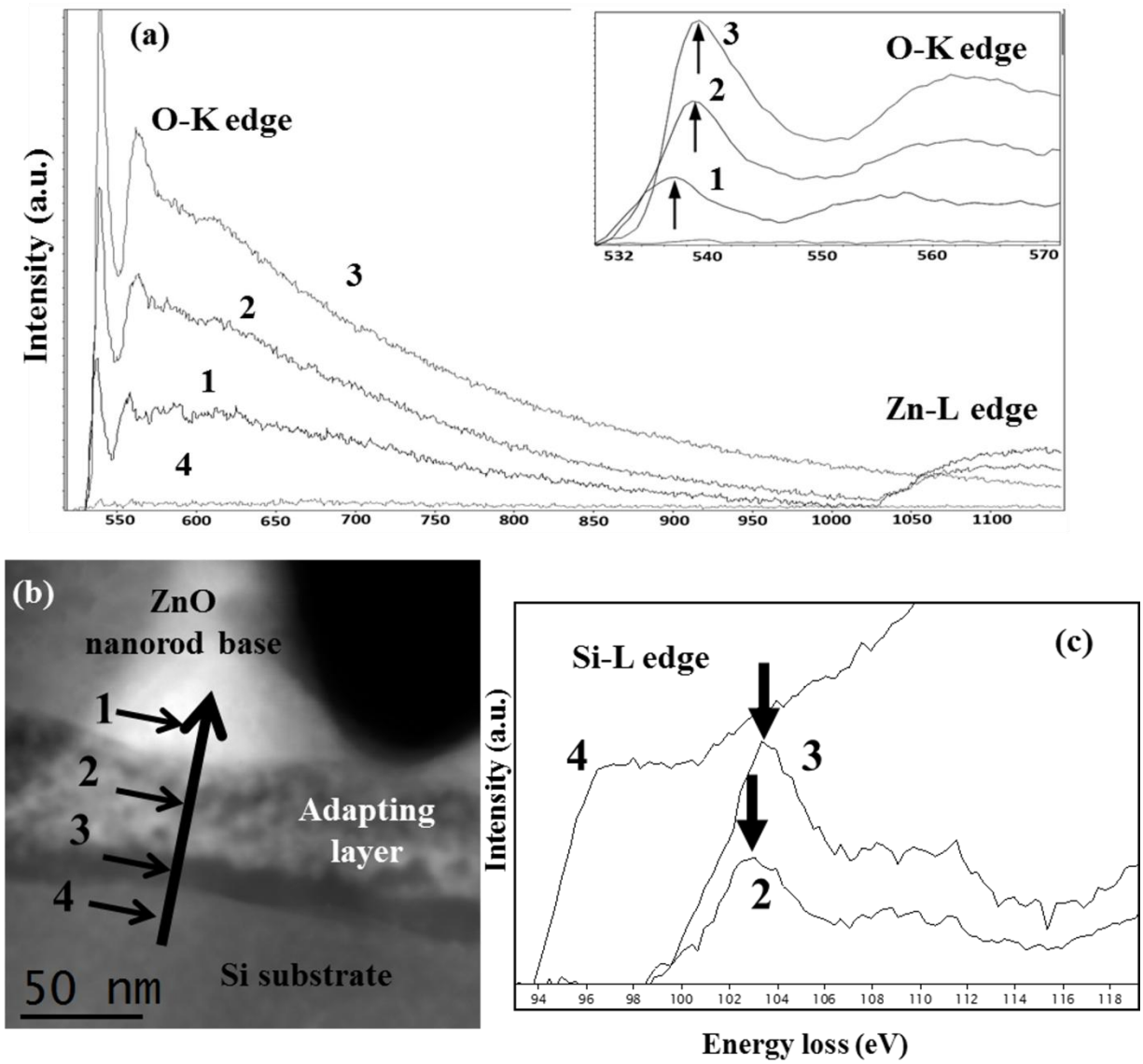

Figure 3. (a) Individual core loss EEL spectra from several points at the Si substrate/nanorod interface in the case of sample B, which are labeled in (b). (b) HAADF-STEM image of this region. The points 1-4 correspond to the ZnO rod base, $Zn_xSi_{1-x}O_y$, SiO_2 layers and Si substrate, respectively. (c) Different Si-L signals recorded for this area.

3.3. Effect of the high VPT temperature on the CBD buffer layers

Through a comparison between samples B and A, we appreciate significant changes in the morphology close to the base and in the structure of the interlayer between the nanorods and the substrate. To establish firstly the effect of these high temperatures on the silica amorphous layer and its influence on the development of the rods, a post-annealing at a temperature similar to that used in the VPT process (but without Zn source materials) was carried out on CBD1 (only with the seed layer) and CBD1 + CBD2 (with CBD nanorods) samples. This treatment should allow us to clarify the processes leading to the alteration of the structural and compositional distribution of both ZnO rods and their interface with the substrate. Firstly, we analyse the effect of the VPT-level temperatures on original CBD1 seed layers. Figure 4a shows a seed layer annealed at 925C° without source material, and the formation of a thick amorphous material over the silicon substrate is seen, whose thickness oscillates between 25 and 40 nm. It is well-known that at high temperatures silicon wafers are oxidized, forming much thicker oxide layers than the native oxide present. HRTEM images of this area revealed particles immersed in an amorphous matrix on the atomically flat Si substrate surface. The sizes of these particles, extracted from the histogram of Figure 4(c), are significantly larger than those seen in seeded samples [17], which suggests that crystal coalescence may also be taking place. A very important finding is that this treatment has a dramatic effect on the ZnO crystallites and seems to render the small seed crystals inactive as potential nucleation sites for subsequent nanorod growth, due to a silica layer overgrowth which covers the particles. That is consistent with experimental observations concerning the difficulty of direct VPT growth on such seed layers [17]. Furthermore, our result suggests that the buffer layer must have a maximum thickness in relation to the particle size during any heat

J. Nanosci. Lett. 2013, 3: 2
www.simplex-academic-publishers.com
© 2012 Simplex Academic Publishers. All rights reserved.

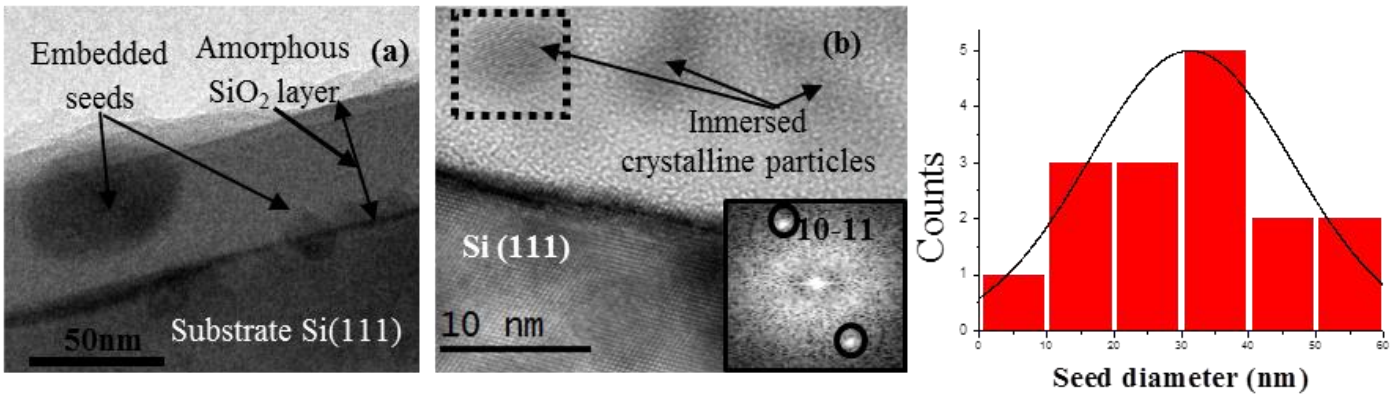

Figure 4. (a) CTEM image of sample which has undergone CBD1+ annealing at 950ºC showing particles embedded within an amorphous layer consisting of SiO_2. (b) HRTEM image detailing the area between the Si substrate and SiO_2 layer, inset FFT of the particle highlighted in the square region in image (b) displays spots associated with planes of Zn_2SiO_4 [19]. (c) Histogram showing the diameter distribution of particles, in particular diameters between 10 and 50 nm with a maximum at 35 nm.

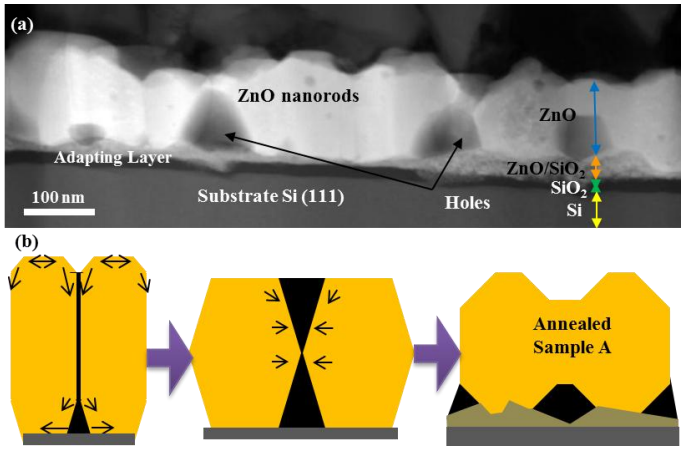

Figure 5. (a) HAADF-STEM image in cross-section view of the substrate/rods interface showing the adapting layer of annealed A-type sample. (b) Schematic representation illustrating the morphological changes among samples A before and after annealing.

treatment to prevent the SiO_2 overgrowth, and the subsequent inhibition of nanorod nucleation.

EDX signals coming from seeds show a ZnO/SiO_2 mixed composition, where the silicon signal is always present due to the finite resolution of the probe beam and the small size of the embedded seeds. In addition, the corresponding FFT of the HRTEM image (see inset of Figure 4b), again shows interplanar distances associated with the Zn_2SiO_4 structure. Thus we cannot ignore the chemical reactions that occur between the ZnO material and the SiO_2 layer during the temperature increase, in particular in VPT samples. We therefore conclude that this temperature is sufficient to achieve the formation of $Zn_xSi_{1-x}O_y$ ternary alloys. In fact, similar results concerning formation of Zn_2SiO_4 crystallites and amorphous SiO_2 during annealing treatments have been reported in ZnO/Si systems [21]. Thus, the ZnO–SiO_2 system around 800ºC is easily transformed into a mixed phase including ZnO, Zn_2SiO_4 and an amorphous SiO_2 [22]. In this respect, the transformation of the ZnO seeds to a Zn_2SiO_4 phase could be an additional explanation of the deactivation of the buffer layer, inhibiting development of ZnO nanorod arrays in subsequent growths.

Similarly to the results for the seed layer, the study of the annealing on sample A gives us information about the influence of typical VPT temperatures, not only on the SiO_2 and ZnO reaction, but also on the ZnO distribution in CBD nanorods. The HAADF-STEM image of Figure 5a corresponds to ZnO nanorods of an annealed sample A in a cross-sectional view. This image clearly displays the radical morphological changes undergone by the ZnO rods in comparison with the unannealed sample A. In particular, the base width of these nanostructures increased from 20-40 nm (for the unannealed sample A) to 80-200 nm, with the overall height remaining very similar (160-200 nm). Furthermore the nanorod shape changes from bullet-shaped to a facetted diamond shape. The fact that these bases, which have no external contribution of Zn source vapour, are four times wider than CBD nanorods means that several CBD nanorods are involved in the formation of a single block, thus reducing the rod density. That confirms temperature as the main driving force of changes in sample B, effect detailed in the previous section.

This transformation is activated by the high temperature, whereby Zn and O atoms from the CBD nanorod acquire sufficient energy to sublime and diffuse from the basal planes to prismatic planes, favoring the nanorod base coalescence. As consequence, this coalescence which decreases the energy of system by reducing the free total surface gives rise to an effective quasi-2D growth mode. The horizontal growth has an additional contribution in the case of sample B due to the high vapor pressure of the Zn flux, characteristic of the initial stages of FRTP [23, 24]. Both factors lead to the creation of wide bases, though via different physical routes.

Regarding the region at the interface, HAADF-STEM images of the annealed A-type sample (Figure 5a) make clear that an adapting layer made up by 2 sub-layers and similar to the VPT samples has also appeared. These outcomes suggest us that VPT annealing temperatures is mainly responsible for the formation of the adapting bilayer, yielding a consumption of the Si surface and indicating that the presence of Zn in the

© 2012 Simplex Academic Publishers. All rights reserved.

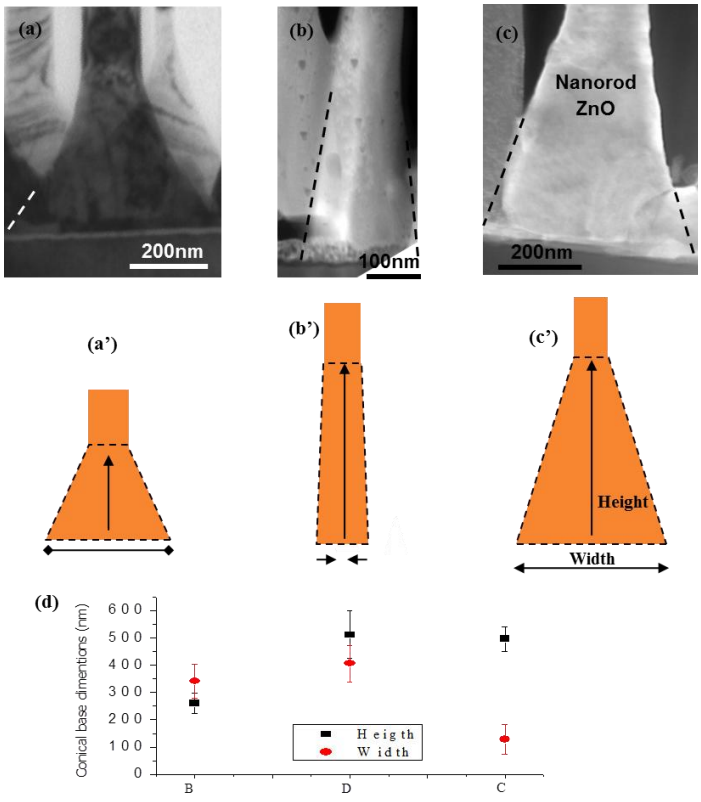

Figure 6. (a), (b) and (c) XTEM images showing the morphology of nanorod bases for samples B, C and D, respectively. (a'), (b') and (c') show a schematic representation comparing the changes for samples B, C and D, respectively, with changes in the VPT process conditions. (d) Graph showing the variation in conical base width and height for samples grown with varying conditions.

adapting layer is not only due to the Zn vapor from the carbothermal reduction reaction, but also from the Zn species in the CBD nanorods (See Figure 5b). Because the Si atom has approximately the same radius as the Zn atom and that the electronegativities of Si (1.9) and Zn (1.65) are both comparable, hence it is easy for Zn to diffuse into SiO_2 in all samples which have undergone the high temperature VPT process or equivalent high temperature anneal, and ultimately to form the Zn_2SiO_4 phase [25, 26]. This layer does not appear in the case of CBD rods, which indicates that the native oxide is not so significantly affected by the CBD process temperatures. Formation of this new adapting layer is in all probability due to the high temperature process employed in these experiments.

3.4. Effects of the VPT temperature ramp rate

As demonstrated in previous sections, the nanorod morphology and the interlayer between the Si substrate and the base of the ZnO nanorod strongly depend on the VPT experimental conditions, Processes such as Zn sublimation and diffusion can be influenced not only by the temperature reached, but also the details of the temperature ramp rate during the VPT step. In this study, another sample, labelled as C, has been produced by the VPT process using the SRTP and compared to sample B (FRTP). Furthermore, an additional sample D was grown following a similar FRTP process but modifying the sample distance to the Zn source (FRTP2). These efforts are intended to elucidate how these parameters affect the composition and morphology of the interlayer below the nanorods and the morphology of the nanorods.

Bearing in mind that the presence of Zn in the adapting layer is not due solely to Zn vapour from the carbothermal reduction reaction, but represents a partial consumption of the CBD deposited rods into the interface, it is important to note that some differences are observed in the adapting layers between samples grown by VPT at different temperature ramp rates. For example, the most uniform interface layer is achieved with the slower temperature ramp rate. This method thus optimises the interface between the substrate and the rod, even more so when comparing with the annealed sample A. Higher temperatures achieved from the beginning of the process on the other hand lead to a more rapid growth of the ZnO/SiO_2 adapting layer, and to the thickest interface layer, as occurs in samples grown by VPT with the FRTP. The most uneven adapting layers are observed in the samples annealed without the source powder suggesting that the Zn vapour has a moderating effect on the gaseous partial pressures leading to a more uniform growth of the SiO_2 interface. Study of these interfaces is very interesting for understanding the growth mechanism of ZnO nanorods. At the nanoscale, the formation of such a complex interlayer between the silicon substrate and the nanorod could influence significantly the electronic and optical properties of the nanorod array. However further work is needed to understand how this layer could affect in luminescence and electrical properties of nanorods grown by this method.

But, probably, more significant are the changes observed in the morphologies of the nanorod bases. Images of the Figure 6 show how the conical bases of the nanorods change their shape depending on both the temperature ramp rate and the position of the substrate with respect to the source material. Using the FRTP with a smaller alumina boat (i.e. sample closer to the source powder), such in the case of sample D, the conical bases appear wider at the bottom and longer compared to other samples prepared using the same FRTP but with substrates further from the powder source (i.e. sample B). By contrast, sample C, grown under the same conditions as the sample B but using the SRTP, has an extended base heights (in length) much greater than sample B. It is worthwhile pointing out however that the conical base widths of sample C have experienced a significant decrease in comparison to sample B or D (see graph in Figure 6d). During FRTP conditions, considerable quantities of Zn vapour contribute to growth at these first stages. In the case of sample D where the source of the material was closer to the silicon wafer, an increased initial Zn vapour concentration during the initial stages of growth occurs giving rise to an extra lateral growth [27]. In the case of sample C, the slow temperature ramp, provides a reduced Zn vapour concentration during the initial stages of growth, thus favouring the 1D growth regimen from the beginning of the growth and hence narrower nanorod bases.

Based on these results, it seems that that through an adequate modulation of the Zn vapour source, we can control the morphology of the nanorod bases.The conical bases are formed by the fusion of several CBD nanorods which are covered with ZnO during the VPT deposition. This coalescence leads to a reduction in final density of nanorods,

© 2012 Simplex Academic Publishers. All rights reserved.

i.e. increased coalescence of CBD rods implies reduced density in VPT nanorods and vice-versa. In this respect sample C shows an improvement with respect to samples B or D, in that the bases of the nanorods are narrower and fewer CBD rods participated in their formation. Thus, density control of ZnO nanorod arrays could be achieved by adjusting the temperature ramp during the VPT, and/or by changing the position of substrate respect to the Zn powder. This fact may be crucial from a technological viewpoint since many applications require a high density of nanorods to improve the device performance and design [28]. Another important feature is that, in spite of the major changes observed in the bases, no significant variation in the diameter of the final VPT nanorods has been observed. The growth parameters seem to have an obvious influence on the base morphology rather than on the upper part of these nanorods. The selection of FRTP (close or far from the source) or SRTP strongly modifies the base morphology, but once the carbothermal reaction reaches an equilibrium, the development of the ZnO nanorods is very similar in all samples.

4. Conclusions

In conclusion, we applied transmission electron microscopy-related techniques to study the effect of the high VPT temperatures during the growth of arrays of ZnO nanorods on silicon substrates using a three step catalyst-free method. The method utilises the formation of an initial ZnO nanorod array using two consecutive CBD processes and subsequent growth thereon via VPT deposition. We have examined the evolution of the interface and the ZnO morphology during each step founding that the main morphological and compositional features of the nanorod arrays depend strongly on the deposition parameters used in the VPT process. Thus, to understand the VPT rod formation, we have considered firstly the effect of annealing buffer layers at temperatures typically reached during the VPT process and secondly, the use of different temperature ramp rates and sample configurations in the VPT deposition. HAADF imaging demonstrated the formation of a double intermediate layer below the base of nanorods with and without Zn supply. HAADF-STEM, HRTEM, EDX and EELS analysis confirmed the presence of a bottom layer of SiO_2 and an upper layer of a mixture of ZnO/$SiO_2$with evidence of ternary compounds of these elements also being formed. Moreover, the VPT process gives rises to the formation of conical shaped structures at the base of the nanorods by the coalescence of several CBD rods whose morphology depends strongly on the VPT experimental conditions. In fact, the conical bases of samples grown closer to the powder source using the FRTP were both the tallest and widest compared to samples grown further from the powder source. This behaviour is explained by 2D growth mode enhancement due to higher levels of Zn supersaturation during the initial stages of the VPT process. Moreover, using SRTP favors 1D growth which gives rise to narrower but taller conical bases. The nanorod top section is developed mainly after a stationary Zn supersaturation level is reached. However, the full details of sublimation and diffusion mechanisms leading to the range of morphological and compositional changes shown by these nanostructures are not fully understood yet. Further studies are needed to understand the phenomena underlying these changes accurately and to pinpoint the main factors involved.

Acknowledgements

Financial support from Spanish project CICYT MAT2010-15206 is gratefully acknowledged. DB and EMCG acknowledge support from Science Foundation Ireland Strategic Research Cluster grant entitled “Functional Oxides and Related Materials for Electronics” (FORME).

References

1. Z. L. Wang, Mater. Sci. Eng. R 64 (2009) 33.
2. Y. Chen, D. M. Bagnall, H.-j. Koh, K.-t. Park, K. Hiraga, Z. Zhu and T. Yao, J. Appl. Phys. 84 (1998) 3912.
3. J. Zhou, N. S. Xu and Z. L. Wang, Adv. Mater. 18 (2006) 2432.
4. Z. Li, R. Yang, M. Yu, F. Bai, C. Li and Z. L. Wang, J. Phys. Chem. C 112 (2008) 20114.
5. D. Bao, H. Gu and A. Kuang, Thin Solid Films 312 (1998) 37.
6. M. Law, L. E. Greene, J. C. Johnson, R. Saykally and P. Yang, Nat. Mater. 4 (2005) 455.
7. L. E. Greene, M. Law, D. H. Tan, M. Montano, J. Goldberger, G. Somorjai and P. Yang, Nano Lett. 5 (2005) 1231.
8. Y. X. Chen, X. Q. Zhao, B. Sha and J. H. Chen, Mater. Lett. 62 (2008) 2369.
9. X. Y. Kong and Z. L. Wang, Nano Lett. 3 (2003) 1625.
10. M. H. Huang, S. Mao, H. Feick, H. Yan, Y. Wu, H. Kind, E. Weber, R. Russo and P. Yang, Science 292 (2001) 1897.
11. Z. L. Wang and J. Song, Science 312 (2006) 242.
12. M. H. Huang, Y. Wu, H. Feick, N. Tran, E. Weber and P. Yang, Adv. Mater. 13 (2001) 113.
13. Z. W. Pan, Z. R. Dai and Z. L. Wang, Science 291 (2001) 1947.
14. C. H. Lu and C. H. Yeh, Ceram. Int. 26 (2000) 351.
15. K. Govender, D. S. Boyle, P. B. Kenway and P. O'Brien, J. Mater. Chem. 14 (2004) 2575.
16. L. E. Greene, M. Law, J. Goldberger, F. Kim, J. C. Johnson, Y. Zhang, R. J. Saykally and P. Yang, Angew. Chem. Int. Ed. 42 (2003) 3031.
17. D. Byrne, E. McGlynn, K. Kumar, M. Biswas, M. O. Henry and G. Hughes, Cryst. Growth Des. 10 (2010) 2400.
18. D. Byrne, E. McGlynn, M. O. Henry, K. Kumar and G. Hughes, Thin Solid Films 518 (2010) 4489.
19. D. R. Lide, CRC Handbook of Chemistry and Physics, CRC Press (1992).
20. S. S. Kim and B.-T. Lee, Thin Solid Films 446 (2004) 307.
21. Y. S. Lim, J. W. Park, M. S. Kim and J. Kim, Appl. Surf. Sci. 253 (2006) 1601.
22. X. Xu, P. Wang, Z. Qi, H. Ming, J. Xu, H. Liu, C. Shi, G. Lu and W. Ge, J. Phys.: Condens. Matter 15 (2003) L607.
23. C. X. Xu, X. W. Sun, Z. L. Dong, G. P. Zhu and Y. P. Cui, Appl. Phys. Lett. 88 (2006) 093101.
24. C. X. Xu and X. W. Sun, Appl. Phys. Lett. 83 (2003) 3806.
25. J. Zhou, J. Liu, X. Wang, J. Song, R. Tummala, N. S. Xu and Z. L. Wang, Small 3 (2007) 622.
26. G. Z. W. H. Q. Wang, L. C. Jia, C. J. Tang, and G. H. Li, J. Phys. Chem. C 111 (2007) 5.
27. R. T. R. Kumar and et al., Nanotechnology 18 (2007) 215704.
28. R. Zhang, S. Kumar, S. Zou and L. L. Kerr, Cryst. Growth Des. 8 (2007) 381.

© 2012 Simplex Academic Publishers. All rights reserved.

Cite this article as:

Rabie Fath Allah *et al.*: **Effect of high temperature VPT conditions on the development of aligned ZnO nanorod arrays grown by a three step catalyst-free method.** *J. Nanosci. Lett.* 2013, **3**: 2

© 2012 Simplex Academic Publishers. All rights reserved.